

ScaleQC: A Scalable Framework for Hybrid Computation on Quantum and Classical Processors*

Wei Tang
 Department of Computer Science
 Princeton University
 weit@princeton.edu

Margaret Martonosi
 Department of Computer Science
 Princeton University
 mrm@princeton.edu

Abstract

Quantum processing unit (QPU) has to satisfy highly demanding quantity and quality requirements on its qubits to produce accurate results for problems at useful scales. Furthermore, classical simulations of quantum circuits generally do not scale. Instead, quantum circuit cutting techniques cut and distribute a large quantum circuit into multiple smaller subcircuits feasible for less powerful QPUs. However, the classical post-processing incurred from the cutting introduces runtime and memory bottlenecks. Our tool, called ScaleQC, addresses the bottlenecks by developing novel algorithmic techniques including (1) a quantum states merging framework that quickly locates the solution states of large quantum circuits; (2) an automatic solver that cuts complex quantum circuits to fit on less powerful QPUs; and (3) a tensor network based post-processing that minimizes the classical overhead. Our experiments demonstrate both QPU requirement advantages over the purely quantum platforms, and runtime advantages over the purely classical platforms for benchmarks up to 1000 qubits.

1 Introduction

Quantum Computing (QC) has been proposed as a promising counterpart to classical computing, but QPUs face demanding hardware requirements to operate at useful scales. Many quantum algorithms offer runtime advantages over the best known classical algorithms, such as unstructured database search [16] and integer factorization [34]. To solve a problem, researchers develop a quantum algorithm that is represented as a n qubit quantum circuit. A QPU then executes the circuit and samples its probability output to find the “solution” states, indicated by their much higher quantum state amplitudes than the non-solution states. In order to even run the circuit at all, the QPU must have at

least n qubits. Furthermore, the QPU’s qubits must be accurate and robust enough to support the quantum workload without accumulating too much noise to produce quality solutions. However, these two requirements put a heavy toll on the hardware. As an example, the famous Shor’s integer factorization algorithm is expected to take millions of physical qubits in order to construct enough number of high quality logical qubits to run problems at practical scales [35].

Instead, the recent introduction of the quantum circuit cutting theory [30] and its early demonstrations [38, 37] hint at the potential to combine multiple less capable QPUs and classical post-processing into a hybrid architecture. Circuit cutting techniques divide a large quantum circuit into several smaller subcircuits, which can be executed in parallel on multiple QPUs with lower qubit quantity and quality requirements. Classical post-processing is then used to reconstruct the output from these small subcircuit outputs. This hybrid architecture is analogous to the classical parallel computing where a large workload is distributed among many computing nodes, which afford to be much less powerful, but at the expense of some communication cost to reconstruct the results.

Dividing a large quantum circuit into many smaller subcircuits introduces obvious advantages over relying on either quantum or classical platforms alone. The most important advantage comes from that the subcircuits usually have fewer quantum gates, potentially also have fewer qubits. This puts a much lower qubit quality requirement for QPUs to produce accurate results, as the shallower and less complicated subcircuits incur much less crosstalk [24], decoherence [20], gate errors [4] and control difficulties [1]. In addition, having fewer qubits directly reduces the strict size limit on QPUs. Specifically, [38] demonstrates that certain algorithms can be run with fewer than half the number of qubits. Furthermore, since QPUs operate much faster than the classical simulations of quantum circuits, such hybrid architecture offers significant runtime speedup. Overall, quantum circuit cutting techniques combine less powerful QPUs and classical computing to expand the computational

*Code available at: <https://doi.org/10.5281/zenodo.6421908>

reach for both.

Despite the obvious advantages, two key challenges remain to make quantum circuit cutting practical. First, the classical post-processing overhead grows quickly with the number of cuts and bottlenecks the end-to-end workflow, preventing its application to hard-to-cut circuits. Second, the memory overhead to store and compute the state space of quantum circuits still doubles with every additional qubit, preventing its application to large circuits.

This paper overcomes the fundamental runtime and memory scalability difficulties of quantum circuit cutting and makes the hybrid architecture practical. Via an iterative search framework called states merging, ScaleQC offers the ability to locate solution states for arbitrarily large quantum circuits, hence bypassing the classical memory limitations. Via an automatic cut solver, ScaleQC finds high quality cuts suitable for post-processing and generalizes to different benchmarks. Via the compute graph contraction algorithm, ScaleQC reduces the runtime overhead to enable the applications to complicated circuits.

To evaluate the performance, we ran several realistic quantum benchmark algorithms such as QAOA [32], AQFT [5], Maximum Independent Set [32], Supremacy [4] and BV [6]. We demonstrated running quantum circuits of up to 1000 qubits. Our contributions include the following:

1. **Reduce Memory:** Developed a states merging method to efficiently locate arbitrary solution states for large quantum circuits, thus overcoming the classical memory scalability obstacles.
2. **Reduce Runtime:** Developed a Mixed Integer Programming (MIP) solver that automatically finds cuts for large quantum circuits to allow easier classical post-processing, while constrained by user-specified available QPU resources.
3. **Reduce Runtime:** Developed a compute graph contraction algorithm to significantly reduce the classical runtime overhead.

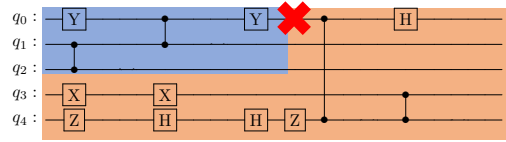
2 Background

This section introduces the quantum circuit cutting theory, its use cases and identifies its key challenges.

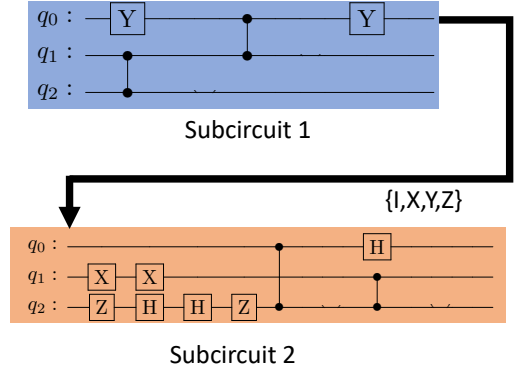
2.1 Circuit Cutting Theory

While we refer the readers to [30] for a detailed derivation and proof of the physics theory, we provide an intuitive understanding of the cutting process in order to identify its key challenges.

Circuit cutting cuts between quantum gates and decomposes the qubit states into their Pauli bases. With a proper



(a) The red cross indicates the cutting point. Subcircuit 1 is shaded blue and subcircuit 2 is shaded orange.



(b) The black arrow between the subcircuits shows the “path” undertaken by the qubit line being cut. The one cut needs to permute each of the $\{I, X, Y, Z\}$ bases. Subcircuit 1 needs to be measured in each basis and subcircuit 2 needs to be initialized in each basis. The two subcircuits can now be executed independently on 3-qubit QPUs.

Figure 1: Example of cutting a 5-qubit quantum circuit with 1 cut that divides it into two smaller subcircuits.

selection of the cutting points, a large quantum circuit can be divided into smaller isolated subcircuits. Figure 1a shows an example 5-qubit quantum circuit. Without cutting, this circuit requires a QPU with at least 5 good enough qubits to execute all the quantum gates before too many errors accumulate. Circuit cutting makes 1 cut and divides this quantum circuit into two smaller subcircuits, each with both fewer qubits and fewer gates. Figure 1b shows that each subcircuit needs to be measured and initialized in different bases according to the permutations of all the cuts. Now multiple less powerful 3-qubit QPUs can run these independent subcircuits in parallel. The quantum interactions among the subcircuits are substituted by classical post-processing, which are analogues to the communication cost paid in classical parallel computing.

In general, a n qubit quantum circuit undergoes K cuts to divide into n_C completely separated subcircuits $C = \{C_1, \dots, C_{n_C}\}$. A complete reconstruction of the quantum interactions requires each cut to permute each of the $\{I, X, Y, Z\}$ bases, for a total of 4^K assignments. Depending on the basis assigned to the cuts connecting each

subcircuit, it is initialized and measured slightly differently to produce a distinct entry. We use $p_i(k)$ to represent the output of subcircuit i in the k th cuts assignment, where $i \in \{1, \dots, n_C\}$ and $k \in \{1, \dots, 4^K\}$. The physics theory [30] dictates that the output of the original circuit is given by

$$P = \sum_{k=1}^{4^K} \otimes_{i=1}^{n_C} p_i(k) \in \mathbb{R}^{2^n} \quad (1)$$

where \otimes is the outer product between two subcircuit output vectors. Note that each subcircuit only has a different entry when at least one cut connecting it in the compute graph changes basis. This means that many of the $p_i(k)$ repeat in the various summation terms.

2.2 Circuit Cutting Use Cases

Several theory proposals [9, 30] first introduce the possibility of quantum circuit cutting. Many small-scale demonstrations exist for chemical molecule simulations [12] and variational quantum solvers [46]. In addition, several quantum computing industry leaders such as IBM and Xanadu [44] are actively developing quantum circuit cutting products. These efforts either apply the hybrid architecture to real-world problems, or aim at incorporating it into the existing quantum hardware and software stack. However, none of the current efforts addresses the scalability obstacles.

2.3 Circuit Cutting Challenges

The key challenges of applying quantum circuit cutting at useful scales lie with the classical post-processing. Equation 1 clearly shows the two challenges as the following:

1. The length of the full output of a n -qubit circuit is 2^n . Large quantum circuits quickly bottleneck the classical memory as well as the runtime.
2. The classical post-processing scales exponentially with the number of cuts required K and hence bottlenecks the runtime.

This paper develops the states merging technique to bypass the memory challenge altogether while reducing the classical overhead. In addition, this paper proposes compute graph contraction to significantly reduce the runtime overhead.

3 Framework Overview

Algorithm 1 outlines the overall framework of ScaleQC. The input to the framework includes the quantum circuit itself and a list of hyperparameters:

Algorithm 1: ScaleQC Framework

Input: Quantum circuit C . Max load factor α . Max number of probability bins allowed per recursion M . Max number of recursions R .

- 1 Initialize an empty list L
- 2 Recursion counter $r \leftarrow 0$
- 3 Find cuts for C to satisfy the max load α and produce the compute graph G . // Section 5
- 4 $n_i \leftarrow$ number of data qubits in subcircuit $i \in \{1, \dots, n_C\}$
- 5 **while** $r < R$ **do**
- 6 **if** $r > 0$ **and** *bin is None* **then**
- 7 **BREAK** // All solution(s) are found
- 8 Compute the bin assignments for each subcircuit // Algorithm 2 [$r, bin, M, n_{1..n_C}$], Section 4
- 9 **QPU** : Run the subcircuits to produce the merged probability bins for the subcircuit $\{p_{i,k}\}$
- 10 Contract the compute graph G to reconstruct the probability sums for the bins // Section 6
- 11 Append the R largest bins not yet fully expanded to L
- 12 Sort and truncate L to keep the largest R bins
- 13 Pop *bin* from L
- 14 $r \leftarrow r + 1$
- 15 **end**

1. Max QPU load factor α : The maximum fraction of the two-qubit gates each QPU can handle. For example, $\alpha = 0.5$ for a quantum circuit with 100 two-qubit gates means ScaleQC needs to cut into subcircuits with at most 50 two-qubit gates.
2. Max per-recursion bins M : The maximum number of probability bins each states merging recursion computes.
3. Max recursions R : maximum number of states merging recursions to run.

The framework is mainly built around an iterative procedure called the states merging to locate the solution states for the input quantum circuit (the *while* loop in ALgorithm 1). Section 4 discusses the iterative procedure in detail. On a high level, ScaleQC recursively evaluates the subcircuits with QPUs and searches the solution states with classical computing until all solution states are found, or the user-defined max recursion depth R is reached first. States merging narrows down to a range of possible states containing the solutions when the max recursion depth is reached

Algorithm 2: States Assignment**Goal:** Reduce memory overhead.

Input: $r, bin, M, n_{1\dots n_C}$ // Refer Algorithm 1

- 1 **if** $r = 0$ **then**
- 2 Initialize each quantum state in its own bin for
 $l_i \leftarrow 2^{n_i}$ bins in subcircuit $i, i \in \{1, \dots, n_C\}$
- 3 **else**
- 4 Locate the subcircuit states contained in bin ,
 $l_i \leftarrow \#states_i$
- 5 Copy $l'_i \leftarrow l_i$
- 6 Initialize the total number of bins required $l \leftarrow \prod_i l'_i$
- 7 **while** $l > M$ **do**
- 8 Pick the subcircuit i with the largest l'_i
- 9 $l'_i \leftarrow \lceil l'_i/2 \rceil$
- 10 $l \leftarrow \prod_i l'_i$
- 11 **end**
- 12 **for** $i \in \{1, \dots, n_C\}$ **do**
- 13 Initialize l'_i empty bins
- 14 **for** $j = 1, \dots, l_i$ **do**
- 15 $k \leftarrow j \% l'_i$
- 16 Append the j th state of subcircuit i to bin k
of subcircuit i
- 17 **end**
- 18 **end**
- 19 **return** *Updated subcircuit bin assignment*

first.

While one can easily use a lot of cuts to separate a large circuit to satisfy the size constraints, the scalability and efficiency of the post-processing largely rely on the strategic choice of the cutting points. Section 5 discusses the MIP solver used to find high quality cuts for any input quantum circuits. Applying the cuts to the input quantum circuit then produces a compute graph abstraction for post-processing.

Quantum and classical platforms then use the compute graph generated from the cuts to reconstruct the original quantum circuit output. Section 6 establishes the classical post-processing of circuit cutting as tensor network contractions, and hence introduces a compute graph contraction method running on GPUs for an efficient classical post-processing.

4 States Merging

Quantum algorithms can be loosely characterized as two groups based on the type of their output. The first type produces concentrated outputs, where a few solution states have much higher probability amplitudes than the others. The solution states should only occupy a very small part of the entire state space, which is the very reason that it is use-

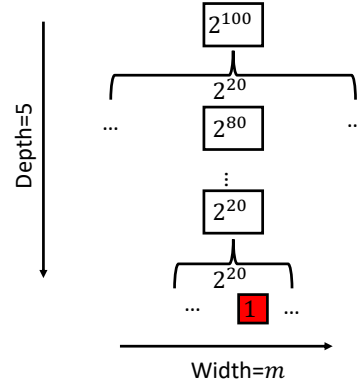


Figure 2: States merging locates solution states for a 100-qubit circuit, with $M = 2^{20}$. Each box represents a bin. The boxed numbers represent the number of quantum states in the bin. Each bracket represents a recursion. The numbers on the brackets indicate the number of bins for the recursion. The red box represents a solution state found.

ful for the quantum algorithms to find them efficiently. This paper mainly focuses on demonstrating circuits of this type.

The second type of algorithms produces a certain probability distribution, where the probability amplitudes are much more distributed among the states. We argue that large size circuits of this type are not practical, since their probability distributions most likely require exponentially many shots to converge even with a large and reliable QPU. In addition, it is impossible to store or analyze the entire state space. As a result, they are usually limited at medium sizes. ScaleQC is able to produce the full state output for this type of circuits.

One major bottleneck of quantum circuit cutting is that the length of the probability output of a n -qubit quantum circuit is 2^n . Hence, full state reconstruction for large circuits quickly increases both the memory requirements and runtime. As an alternative, states merging offers a scalable way to only locate the solution states for large circuits.

The states merging method makes use of the fact that the individual probabilities of the non-solution states are not of interest. Hence, instead of keeping track of the individual probability for each quantum state, the states merging method merges multiple states into one bin and keeps track of their sum of probabilities. The bins containing the solution states hence have much higher probabilities than the other bins and can be easily identified. The *while* loop in the ScaleQC framework in Algorithm 1 shows the complete process.

Each recursion of the procedure first assigns the quantum states still under analysis into various bins. Algorithm 2 shows the assignment process. Lines 1-4 first calculate the current number of bins for each subcircuit. The first recur-

sion starts with each quantum state in its own separate bin, hence each subcircuit has $l_i = 2^{n_i}$ bins, where n_i is the number of data qubits in the subcircuit i . Subsequent recursions seek to expand a particular selected *bin*, hence each subcircuit has the number of subcircuit states belonging to the selected *bin*.

Next, lines 6-11 calculate the target number of bins to use for the next recursion. We shrink the subcircuit with the most number of bins by 2. The shrinking steps repeat until the total number of bins required satisfies the given memory limit M .

Finally, lines 12-18 evenly assign the quantum states under analysis into the number of bins calculated for the next recursion.

The max number of bins M enables a key trade-off for the states merging procedure. The states merging procedure is equivalent to a full state reconstruction if the max number of bins allowed M is larger than the size of the full state 2^n . In this case, the states merging procedure simply locates all the solution states in one recursion. Any M smaller than 2^n essentially provides a trade-off of the size of the vectors to compute during each iteration versus the number of iterations required to locate all the solution states.

For the extreme case where the non-solution states have 0 probability, the states merging procedure is guaranteed to find all the solutions in at most $mn/\log_2 M$ recursions for a n -qubit circuit. Where m is the number of solution states. Figure 2 visualizes an example for a 100-qubit circuit, assuming $M = 2^{20}$ bins, which is negligible as compared to the 2^{100} full states. Each recursion expands a bin for finer details of the quantum states contained. A max depth of $\frac{100}{20} = 5$ produces leaf bins with just 1 state. A solution state is found when a leaf bin with just 1 state and high probability is computed. The entire states merging process hence creates a search tree with a depth of $n/\log_2 M$ and width of m , representing total $mn/\log_2 M$ recursions.

The procedure finds solutions more quickly if multiple solution states happen to be assigned into the same bin, which reduces the width of the search tree at some depth. Having larger M shortens the search tree but has diminishing returns, as doubling M only increases the denominator by 1. Furthermore, larger M means slower post-processing for each recursion. As a result, it is usually favored to use smaller M even if larger M fits in the memory.

In addition, larger quantum circuits (larger n) and more solution states (larger m) only increase the number of states merging recursions linearly. The method hence easily scales to large quantum circuits with more solution states.

Comparison with classical arbitrary state simulation methods: The state-of-the-art simulation work [22] only simulates an arbitrary subset of quantum states for large circuits to avoid the exponential number of quantum states. Our method easily achieves the same functionality if we

just select an arbitrary subset of quantum states to run for a single recursion without merging into bins. However, such arbitrary selection methods will have virtually 0 chance to include any solution states in the sampled subset. To find any solution states, such methods will need to run almost 2^n times and thus do not scale. Instead, the states merging method strictly outperforms the existing methods via its iterative searches.

[38] proposed a Dynamic Definition search method that is similar in spirit with states merging. The method iteratively fixes the state of the individual qubits to search for the solution states. However, this method forces quantum states without common qubit states (such as $|01\rangle$ and $|10\rangle$) to be in different bins, thus can only be located in separate recursions. States merging is hence more efficient as it allows any solution states to be located simultaneously.

5 Locate Cutting Points

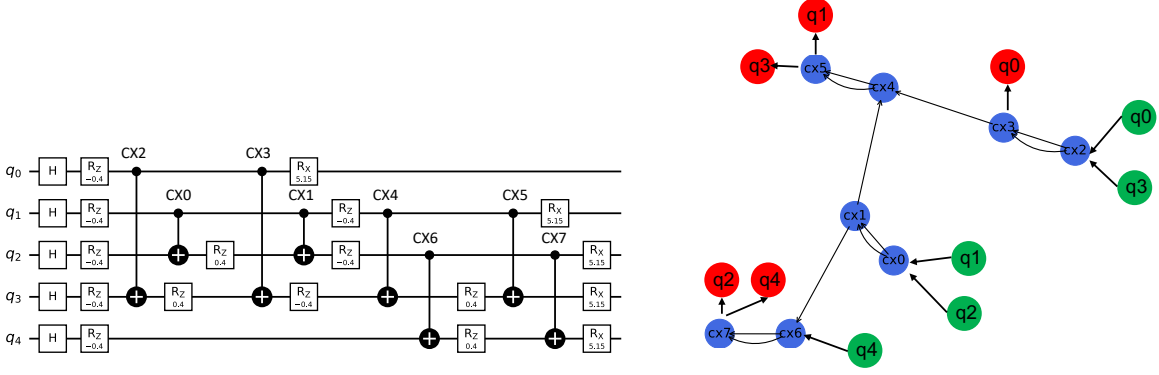
With the overall framework in mind, this section discusses the first step in circuit cutting – determine the cutting points.

Figure 3a shows an example QAOA quantum circuit solving the maximum independent set problem for a random Erdos-Renyi graph with 5 qubits. Quantum circuits can also be represented as directed acyclic graphs (DAG), where the vertices are the gates and the edges are the qubit lines connecting the gates. Hence, locating the cutting points is equivalent to partitioning the quantum gates into certain number of subcircuits. Note that DAG partition problems only concern with the connection among the vertices, but the single qubit gates do not affect such connections. As a result, the single qubit gates are ignored during cuts finding, and are simply attributed to the same subcircuit as their closest two-qubit gate neighbor.

Figure 3b shows its corresponding DAG representation after removing the single-qubit gates. The input (green) and output (red) qubit vertices are illustrated for a clearer correspondence with Figure 3a. However, there is no reason to partition any I/O vertices solely by themselves. Therefore, the I/O vertices are also safely ignored during cuts finding.

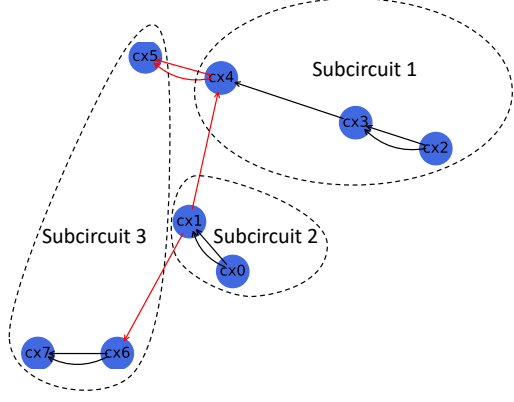
5.1 MIP Model

Figure 3c shows the DAG graph to partition, which only includes the two-qubit quantum gates. We adapt from [38] to encode the DAG for our MIP solver. We denote the n_C subcircuits as $\{C_1, \dots, C_{n_C}\}$, all the qubit lines as edges in E , and all the quantum gates as vertices in V . Furthermore,

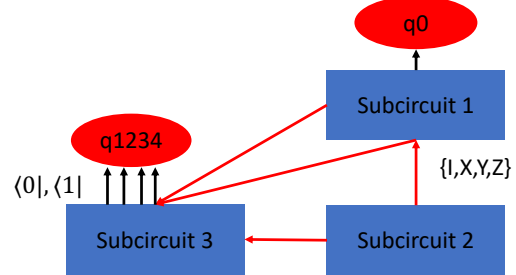


(a) Quantum circuit. Each horizontal line is an input qubit. Time goes from left to right. The indices on the two-qubit CX gates map across the subfigures.

(b) DAG representation of 3a without the single-qubit gates. The green vertices indicate the input qubits. The red vertices indicate the output qubits. The blue vertices indicate the two-qubit quantum gates. The directed edges indicate the time flow of the qubit lines. Qubits in the initial states (green) go through the quantum gates (blue) and measured as output (red).



(c) We only consider the blue quantum gates from 3b for the DAG partition problem. The red edges indicate the cuts found by our solver, subject to $\alpha = 0.4$ max load constraint, i.e. 3 two-qubit gates.



(d) Compute graph abstraction. The cut (red) edges among the subcircuits are the indices to be contracted. The output qubit (black) edges are the output indices.

Figure 3: QAOA benchmark circuit solving the maximum independent set problem for a random Erdos-Renyi graph with 5 qubits.

we define the edge and vertex variables as

$$x_{e,c} \equiv \begin{cases} 1 & \text{if edge } e \text{ is cut by subcircuit } c \\ 0 & \text{otherwise} \end{cases}$$

$$y_{v,c} \equiv \begin{cases} 1 & \text{if vertex } v \text{ is in subcircuit } c \\ 0 & \text{otherwise} \end{cases}$$

$\forall e \in E, \forall v \in V, \forall c \in \{1 \dots n_C\}$

The numbers of incoming and outgoing cut edges to a

subcircuit are modeled as

$$I_c = \sum_{e \in E} x_{e,c} \times y_{e[1],c}$$

$$O_c = \sum_{e \in E} x_{e,c} \times y_{e[0],c}$$

The number of quantum gates in each subcircuit is modeled as

$$S_c = \sum_{v \in V} y_{v,c}$$

5.2 MIP Constraints and Objective

Figure 3d shows the subcircuit abstraction obtained after applying some cuts to the DAG. We call this abstraction the compute graph, where each subcircuit is a vertex and the edges are the cuts selected. Each subcircuit is also connected with some output qubit vertices. We limit the max subcircuit size based on the load factor α and demand that

$$S_c \leq \alpha|V|, \forall c \in C \quad (2)$$

In addition, the MIP model contains the corresponding constraints to help define the edge and vertex variables.

Our efficient post-processing algorithms escape the seemingly exponential cost suggested by Equation 1, but they also make the exact post-processing cost of quantum circuit cutting much nuanced and depend on many factors. We defer the detailed discussions of post-processing the compute graph to Section 6, specifically its cost in Section 6.2. Let us accept for now that the computation complexity is closely related with the compute graph degree, which serves as an indirect measure of the computation overhead. The compute graph degree is just the max number of cuts on any subcircuit, which is simply the sum of the incoming and outgoing cut edges. Therefore, our MIP solver seeks to minimize

$$L \equiv \max_{c \in \{1 \dots n_C\}} \{I_c + O_c\} \quad (3)$$

Furthermore, the number of subcircuits n_C to partition into cannot be captured as part of the optimization model. Instead, we run our solver for up to n subcircuits for a n -qubit benchmark to obtain several possible solutions. Results from Section 6 then allow us to predict the exact post-processing cost for each. The cutting solution with the lowest computation cost is eventually selected.

Overall, the cut search problem is transformed as an integer programming model. However, this constrained graph partition problem is conjectured to have no efficient solutions in polynomial time [2]. Instead, we utilized the commercial solver Gurobi [17] to implement our model. We limit the runtime to 30 seconds for each candidate n_C for an approximate solution if an optimal solution is not found within the time.

6 Compute Graph Contraction

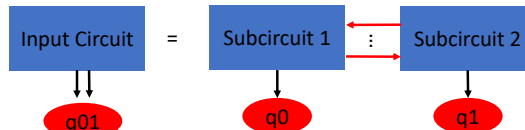
This section introduces compute graph contraction for an efficient post-processing. According to Equation 1, the final reconstruction of the output of the uncut circuit requires permutating the $\{I, X, Y, Z\}$ indices for the K cut edges, taking the outer products among the subcircuits, and sum over all the 4^K terms. The naive computation of Equation 1

$$i \text{---} C \text{---} k = i \text{---} A \text{---} j \text{---} B \text{---} k$$



$$C_{i,k} = \sum_j A_{i,j} B_{j,k}$$

(a) Contracting a pair of tensors means taking the sum over their common index (indices).



$$P = \sum_{k=1}^{4^{\#cuts}} p_1(k) \otimes p_2(k)$$

$$\rightarrow P_{q_0, q_1} = \sum_k p_1(k, q_0) p_2(k, q_1)$$

(b) Contracting a pair of subcircuits is equivalent to tensor contraction. Each cut edge has a dimension of 4, each output qubit has a dimension of 2.

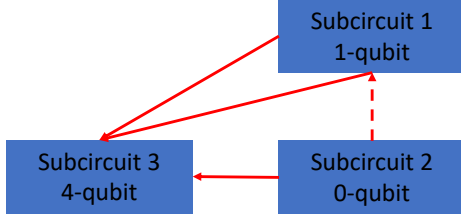
Figure 4: Contracting two subcircuits is equivalent to a pair of tensor contraction.

quickly becomes the bottleneck for complicated circuits as it incurs many redundant computations. This is because subcircuits in general do not connect with all the edges and hence remain unchanged across many different edge bases. In addition, it is preferable to group many outer products as matrix products, as GPUs usually compute matrix products much faster than the explicit iterations over the rows and columns. Compute graph contraction hence seeks to eliminate the redundant computations and exploit the more efficient compute kernels.

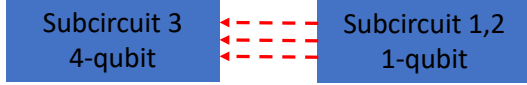
6.1 Relation with Tensor Network Contraction

Post-processing the compute graph is in fact equivalent to tensor network contractions, which have been widely used in classical simulations of quantum systems [41, 42, 33, 40]. Figure 4 establishes the equivalence of a pairwise tensor contraction with a compute graph contraction containing two subcircuits.

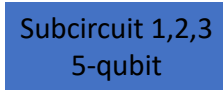
Figure 4a shows contracting a pair of tensors, which are simply multi-dimensional matrices. It hence represents contracting a tensor A of shape $\text{dim}(i)$ -by- $\text{dim}(j)$ with a tensor B of shape $\text{dim}(j)$ -by- $\text{dim}(k)$ to produce a tensor C of shape $\text{dim}(i)$ -by- $\text{dim}(k)$, where $\text{dim}(\cdot)$ is the dimension of an index. By examining the definition of the resulting tensor C , it is easy to verify that a pairwise tensor contraction



(a) Contracting subcircuits 1, 2. Subcircuit 1 tensor has dimensions of $\{4, 4, 4, 2^1\}$. Subcircuit 2 tensor has dimensions of $\{4, 4, 2^0\}$. Subcircuit 3 tensor has dimensions of $\{4, 4, 4, 2^4\}$.



(b) Contracting subcircuit 3 with the already contracted subcircuits 1, 2.



(c) Contraction process finishes. The output is a single tensor of dimension $\{2^5\}$, as expected from a 5-qubit input circuit.

Figure 5: Contracting the compute graph example from Figure 3d. The output qubits are abbreviated as the number of qubits in each tensor for brevity. The dashed edges are the contraction edges in each step. The sub-figures show the best contraction order obtained from Section 6.4.

is simply the matrix product $C = AB$.

Figure 4b shows a hypothetical example of contracting a compute graph with two subcircuits. Each subcircuit is a tensor, the cut edges are the common indices to be contracted, and the output qubits are the output indices. Each cut edge has a dimension of 4 because of the $\{I, X, Y, Z\}$ labels to permute. Each output qubit has a dimension of 2 because of the $|0\rangle, |1\rangle$ bases. Explicitly writing out the output indices based off Equation 1 clearly shows that the compute graph contraction is exactly a tensor contraction.

Figure 5 shows the contraction process for the compute graph in Figure 3d as tensor contractions. Each subcircuit has different number of cuts and number of qubits, hence different dimensions of tensors at the beginning. Each step contracts two vertices in the compute graph. The contraction process finishes when all the vertices are contracted into a single vertex. The final output of compute graph contraction is a single tensor of dimension $\{2^n\}$ for a n -qubit circuit when using full state reconstruction.

Furthermore, when we apply states merging to large circuits beyond classical memory, the beginning tensors have their last dimensions as however many bins each subcircuit

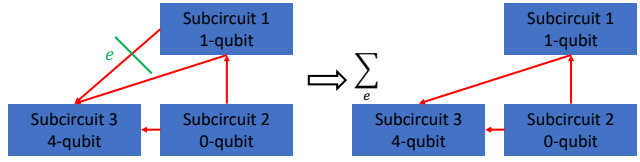


Figure 6: Slicing one cut edge to express the compute graph as a summation of smaller compute graphs.

has. The final output of compute graph contraction is instead a single tensor of dimension $\{M\}$.

6.2 Memory Requirement and Compute Cost

The memory requirement of the post-processing comes from two parts. First, we need to store the input subcircuit tensors. The tensor of subcircuit i has $4^{\#cuts_i} \times 2^{\#qubits}$ ($4^{\#cuts_i} \times \#bins_i$) floats when employing full state (states merging). Second, we need to store all the intermediate tensor products during the contraction.

The compute cost of the post-processing can be captured by the floating point multiplications required in all the contraction steps. The number of multiplications of a pair of contraction is simply the product of all the dimensions involved. For example, Figure 4a requires $\dim(i) \times \dim(j) \times \dim(k)$ multiplications. Similarly, Figure 4b requires $2^1 \times 4^{\#cuts} \times 2^1$ multiplications.

Now we can easily predict the memory and compute overhead of a compute graph without actually performing the computations. The input subcircuit tensors for the example contraction step in Figure 5a require total $4^3 \times 2^1 + 4^2 \times 2^0 + 4^3 \times 2^4 = 1168$ float numbers and $(4^2 \times 2^1) \times (4^1) \times (4^1 \times 2^0) = 512$ multiplications. The contraction step in Figure 5b requires $4^3 \times 2^4 + 4^3 \times 2^1 = 1152$ float numbers and $2^4 \times 4^3 \times 2^1 = 2048$ multiplications.

In contrast, the naive computation of Figure 5a based on Equation 1 requires $4^4 \times (2^1 \times 2^0 + 2^1 \times 2^4) = 8704$ multiplications, a $3.4\times$ extra overhead.

It is now clear that both the memory and compute cost of compute graph contraction are positively correlated with the number of cuts on each subcircuit during every contraction step. This explains our MIP solver objective choice in Equation 3. In order to keep the post-processing runtimes reasonable, we limit the compute graph degree to be 15.

6.3 Two Level Index Slicing

It is possible that complicated compute graphs with many cuts require input subcircuit tensors too large to fit in the memory. Hence we implement an index slicing strategy

prior to their contraction to reduce the input tensor sizes. Index slicing is to explicitly write out certain indices and express the full tensor network as a summation of smaller tensor networks. In the context of compute graph, it is to explicitly write out certain cut edges. For example, slicing one edge in Figure 6 reduces the input subcircuit tensor sizes to $4^2 \times 2^1 + 4^2 \times 2^0 + 4^2 \times 2^4 = 304$ float numbers but produces 4 smaller compute graphs to contract. Our heuristics keep slicing the index that reduces the overall tensor sizes the most, until the overall sizes fit in the memory specified. The heuristics hence produce a set of smaller compute graphs that we explicitly iterate over.

In addition, the intermediate tensor products during contractions may also exceed memory. We further applied the index slicing algorithm from the CoTenGra software [15] to each sub compute graph generated from the first level of slicing.

6.4 Determine Contraction Order

In tensor network contractions, different contraction orders significantly affect the overhead, sometimes even introduce orders of magnitude differences. In circuit cutting, the contraction order of the subcircuits only affects the reconstruction up to a permutation of the qubit order, and has no effect on the quantum state probability accuracy. However, finding the optimal contraction order for general compute graphs is hard. In fact, it is an active area of research and of broader interest across many disciplines [31, 23, 28]. We used the CoTenGra software [15] to compile the contraction order for each sub compute graph.

7 Methodology

This section introduces the various backends, benchmarks, and metrics.

7.1 Backends

The following three backends are involved in the experiments:

1. Quantum: Direct evaluation of quantum circuits on a powerful enough QPU without circuit cutting;
2. Cut: The standard ScaleQC framework in full state;
3. Cut_M: Cut with states merging. This is equivalent to full state evaluation when states merging runs to completion. We run the max number of $mn/\log_2 M$ recursions to guarantee completion.

Large circuits tend to have larger subcircuits as well, but the Noisy Intermediate Scale Quantum (NISQ) devices

nowadays are still too small and noisy for any meaningful experiments at even medium sizes. Hence we use random numbers as the subcircuit output. Although it does not produce any useful circuit outputs, it does not affect the post-processing runtime results of the experiments. We expect more reliable QPUs to enable a full implementation of the ScaleQC framework.

We use a single compute node with 64 CPUs equipped with a single Nvidia A100 GPU for all the cuts finding and classical post-processing.

7.2 Benchmarks

We used the following circuits as benchmarks:

1. *BV*: Bernstein-Vazirani circuit [6] solves the hidden substring problem. Has 1 solution state.
2. *Regular*: Quantum Approximate Optimization Algorithm solves the maximum independent set problem for random 3-regular graphs [32]. With the proper hyperparameters, this circuit produces 1 solution state. However, the full QAOA training process to solve the hyperparameters is beyond the scope of this paper. We use random hyperparameters with the same circuit structure.
3. *Erdos*: The same algorithm as *Regular* but for random Erdos-Renyi graphs.
4. *Supremacy*: Random quantum circuits adapted from [7]. Deeper versions of the circuit was used by Google to demonstrate quantum advantage [4]. Our paper uses depth $(1 + 8 + 1)$ at various sizes. As it does not have well-defined solution states, we run $mn/\log_2 M$ recursions to produce more samples.
5. *AQFT*: Approximate Quantum Fourier Transform [5] that is expected to outperform the standard QFT circuit under noise.

All of our benchmarks are examples of circuits and routines that are expected to demonstrate quantum advantage over classical computing on the Quantum backend. ScaleQC aims to demonstrate the middle ground where the overall runtime is slower than Quantum but still beyond the classical reach, while the quantum and classical computing resources requirements are much lower.

7.3 Metrics

There are two key metrics this paper looks at, namely runtime and quantum resources.

Runtime, faster is better: For Quantum, it is the end-to-end runtime on a standalone QPU, which is the best runtime possible. The Cut and Cut_M backends are slower.

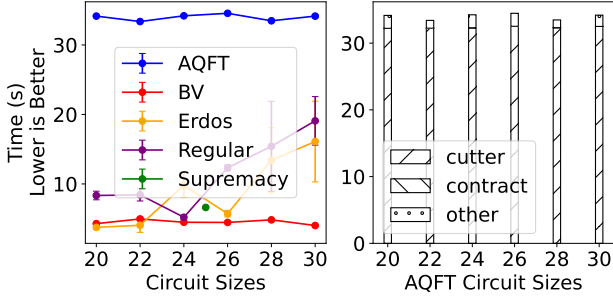


Figure 7: Full state runtimes. Max load $\alpha = 0.4$. Each data point is the average of 5 trials. (Left Panel) The runtimes of 20-30 qubits benchmarks. The error bars represent the standard deviations. (Right Panel) The runtime breakdown for the *AQFT* benchmark. The majority of the runtime is from the cut searching.

The ScaleQC runtime is the end-to-end runtime except time spent on QPUs in Algorithm 1. The NISQ QPUs nowadays are small, slow and too noisy for any practical purposes. As we expect the practical ScaleQC applications to be used with medium sized reliable QPUs in the near future, it is irrelevant to profile the NISQ QPU runtime now. Furthermore, multiple small QPUs can be used in parallel to reduce the runtime. In addition, the runtime advantage of QPUs over CPUs will be even more significant for larger circuits. We expect the framework to offer more significant advantages over classical methods as larger and more reliable QPUs become available.

Quantum Area, smaller is better: The quantum resources requirement is loosely defined as the product of the circuit width and depth, called the ‘quantum area’. Classical simulations require 0 quantum area as it does not use QPUs at all. For Quantum, it is simply the product of the number of qubits and the circuit depth of the input quantum circuit. For the various ScaleQC backends, it is defined for the largest subcircuit produced from cutting. The rationale is that QPUs must be able to support the workloads with a certain quantum area at high accuracy to produce accurate results. While many hardware and software factors affect the QPUs’ ability to support quantum workloads, a smaller quantum area generally puts less burden on the quantum resources.

8 Experiment Results

8.1 Runtime

When the size of the Hilbert space of the quantum circuits is still within the memory limit, it is possible to perform full state evaluation. This cutoff depends on the particular classical backend available to the users. We use

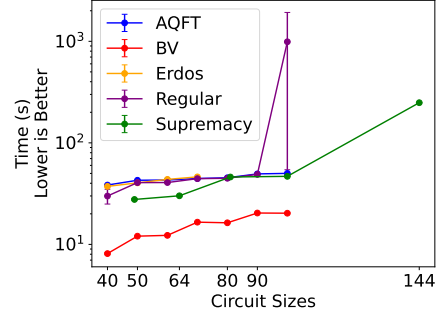


Figure 8: States merging for large circuits. Max load $\alpha = 0.8$ for *Regular* and *Erdos*, $\alpha = 0.5$ for the rest. Max bins $M = 2^{20}$. Each data point is the average of up to 5 trials. Cut_M runs $n/\log_2 M$ recursions (i.e. 5 for the 100-qubit benchmarks) to find at least one solution. Cut_M scales well and is able to run circuits significantly beyond the classical simulation limit.

30 qubits as the cutoff in this paper, which is roughly 10^9 states. However, since each qubit doubles the memory requirement, there is little value in pushing this cutoff point to the extreme.

Figure 7 plots the benchmark circuits 20 \rightarrow 30 qubits, subject to a max load of $\alpha = 0.4$. We observe that the majority of the runtime is spent on searching the cuts. For example, the runtime breakdown of the *AQFT* benchmarks shows that nearly all of the postprocessing runtime comes from the cut searching. This pre-processing overhead can be significant for medium sized benchmarks due to their short overall runtime. As a result, it might not be worth the overhead to use circuit cutting for medium circuits. Admittedly, classical simulators operate relatively fast and are usually adequate for such small benchmarks. As a reference, the widely used Qiskit [3] simulator takes about 30 \rightarrow 50 seconds to run the 30-qubit benchmarks on the same classical backend. ScaleQC is able to produce comparable runtime even for the small benchmarks where classical simulation excels.

While finding the optimal cut solution can be difficult for large circuits, our experiments capped the solver runtime to produce high quality solutions. The cut searching step can hence be viewed as a nearly constant pre-processing overhead for large benchmarks. In fact, ScaleQC has more significant runtime advantages for larger circuits, where the cut searching overhead no longer bottlenecks the framework. Furthermore, ScaleQC with states merging becomes necessary to deal with the exponentially increasing state space.

Figure 8 plots the runtime scalability for large benchmarks, subject to a max load of $\alpha = 0.8$ for the two QAOA benchmarks and $\alpha = 0.5$ for the rest. We set $M = 2^{20}$ bins. Each experiment runs $n/\log_2 M$ recursions to find at least

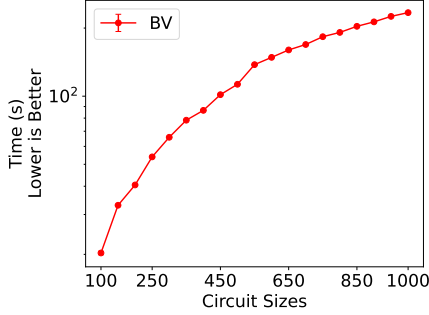


Figure 9: States merging for large BV circuits. Max load $\alpha = 0.5$. Max bins $M = 2^{20}$. Each data point is the average of 5 trials. Cut_M runs $n/\log_2 M$ recursions (i.e. 50 for the 1000-qubit benchmark) to find the unique solution.

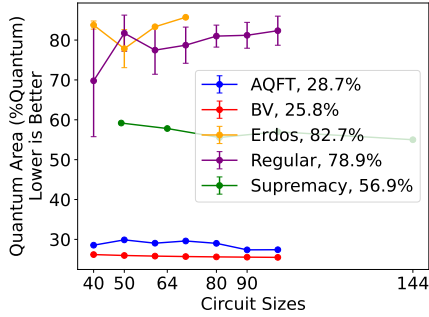


Figure 10: Quantum areas comparisons for the same experiments in Figure 8. The numbers in the legends indicate the average quantum area of Cut_M as a percentage over Quantum. Cut_M requires QPUs to support at most 83% of the quantum area at the expense of the classical runtimes in Figure 8.

one solution. The runtime will be the same to reconstruct $Mn/\log_2 M$ states for the *Supremacy* benchmark, which is about 7 million states for the 144(12×12)-qubit circuit. Instead, states merging obtains more information about the entire state space under the same time.

Figure 9 plots the runtime scalability for the BV benchmark up to 1000 qubits, subject to a max load of $\alpha = 0.5$ and $M = 2^{20}$ bins. Each experiment runs to completion to find the unique hidden string solution state.

The various benchmarks scale well as circuits get larger. The *Erdos* benchmark appears to be the hardest and no solutions were found above 80 qubits for the maximum of 15 compute graph degree.

8.2 Resources Estimations

ScaleQC also requires much less powerful QPUs than Quantum since it just needs to support the smaller subcir-

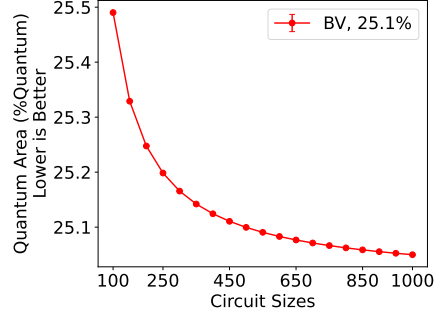


Figure 11: Quantum areas comparisons for the same experiments in Figure 9. Cut_M requires QPUs to support about 25% of the quantum area at the expense of the runtimes in Figure 9.

cuts. Figure 10 plots the quantum areas of Cut_M as the percentage of Quantum for the same experiments in Figure 8. Figure 11 similarly plots the quantum areas of the large BV benchmarks in Figure 9. Quantum simply requires the area of the input benchmark circuit. Cut_M requires QPUs to support the quantum area of the largest subcircuit from cutting. With $\alpha = 0.5(0.8)$, Cut_M requires QPUs to support at most about 57%(83%) of the quantum area to run the various benchmarks, at the expense of the postprocessing runtimes in Figures 8 and 9.

Lower quantum area requirements translate to the ability to tolerate smaller and noisier NISQ devices. Furthermore, in the fault tolerant regime, lower quantum areas translate to a looser requirement on the logical qubit error rate. Depending on different quantum error correction solutions, this implies much reduced physical qubit counts and error threshold requirements. In addition, compiling and decoding the smaller subcircuits are also much easier than larger circuits, which put much less burden on the quantum software development [36].

8.3 Compare Against Classical Simulation

There are lots of purely classical simulation works [43, 10, 18, 29]. The state-of-the-art tensor network based method [22] slices a deeper 100-qubit *Supremacy* circuit into 32^6 “subtasks” to fit onto almost 42 million cores on the Sunway supercomputer. As a comparison, our shallower benchmark will be sliced into 2^6 such “subtasks” by the same metric.

Figure 12 shows a qualitative comparison for the most related benchmark circuit. To maintain their 300 seconds runtime, we estimate [22] to require $42 \times 10^6 \times \frac{2^6}{32^6} \approx 2.5$ cores for 1 million samples at $< 1\%$ fidelity, or $2.5 \times 5 \times 100 = 1250$ cores for 5 million samples at the same perfect postprocessing fidelity as ScaleQC shows in Figure 8.

Method	Supremacy Benchmark	Backend	Runtime	Result
ScaleQC	$10 \times 10 \times (1 + 8 + 1)$ #subtasks = 2^6	1 Nvidia A100 GPU on 1 core.	50 seconds	About 5 million states at perfect classical postprocessing fidelity. Overall fidelity depends on QPUs.
Liu et al.	$10 \times 10 \times (1 + 40 + 1)$ #subtasks = 32^6	42 million cores on the Sunway supercomputer.	304 seconds	About 1 million states at < 1% fidelity.

Figure 12: Compare against [22]. We estimate [22] requires $42 \times 10^6 \times \frac{2^6}{32^6} \times 100 \times 5 \approx 1250$ cores and 300 seconds for our benchmark. Each recursion of ScaleQC produces 1 million more states at minimal extra runtime cost. However, [22] requires the same time for each 1 million more states.

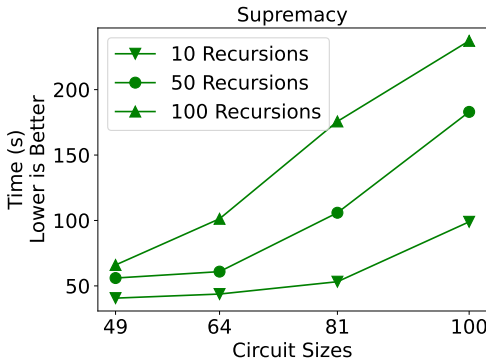


Figure 13: Running the *Supremacy* benchmark for varying number of recursions. Max load $\alpha = 0.5$, max bins $M = 2^{20}$. Since each states merging recursion is fast, adding more recursions do not increase the runtime too much.

We can easily modify the states merging framework to instead produce 1 million arbitrary states in each recursion. Figure 13 runs various *Supremacy* benchmarks for 10, 50, 100 recursions. Specifically, 5 recursions of the 100-qubit *Supremacy* benchmark takes about 50 seconds in Figure 8. Meanwhile, 100 recursions of the same benchmark only takes about 160 seconds in Figure 13. The little runtime increase for more recursions shows that the majority of the runtime is the one-time initial cut searching. Furthermore, the cut searching allows our method to generalize to any benchmarks.

In contrast, [22] manually pre-determines the slicing strategy specifically but only for the *Supremacy* benchmark. It also needs to spend the same runtime for every 1 million more samples calculated.

Deeper and more complicated benchmarks are going to require more than a single GPU. ScaleQC relies on the continued developments of HPC techniques to port to scalable

parallel computing backends.

9 Related Work

Many quantum compiler works exist to improve the performance of standalone QPUs to evaluate quantum circuits [27, 36, 25, 11, 26]. Quantum error correction is the key to build reliable QPUs [14, 8, 19, 45, 21]. QAOA uses classical computing to tune quantum circuit hyperparameters to solve optimization problems [13, 39]. However, they still rely entirely on QPUs to compute the quantum circuits.

Prior circuit cutting implementations [38, 37] rely on parallelization techniques for faster compute while performing direct reconstruction of Equation 1 with high overhead. The various post-processing algorithms proposed in this paper go beyond what is possible from such techniques and reduce the overhead itself.

10 Conclusion

This paper overcomes the classical runtime and memory scalability challenges for hybrid computation via novel post-processing algorithms and develops the corresponding cuts searching algorithm. By distributing large quantum workloads to quantum and classical processors, we demonstrate up to 1000-qubit quantum circuits running on both QPUs and GPUs, which is significantly beyond the reach of either platform alone and previous hybrid workflows. As ScaleQC bridges the classical and the quantum technologies and paves the way for hybrid computations, its future developments naturally benefit from advancements on both sides.

Acknowledgements

We thank Johnnie Gray, Stojche Nakov, Naorin Hossain, François Pellegrini and George Bosilca for helpful discussions and feedback.

Funding acknowledgements: This work is partly funded by EPiQC, an NSF Expedition in Computing, under grants CCF-1730082/1730449. This work is partly based upon work supported by the U.S. Department of Energy, Office of Science, National Quantum Information Science Research Centers, Co-design Center for Quantum Advantage (C2QA) under contract number DE-SC0012704. This material is based upon work supported by (while Martonosi was serving at) the National Science Foundation.

References

- [1] Mohamed Abdelhafez, Brian Baker, András Gyenis, Pranav Mundada, Andrew A Houck, David Schuster, and Jens Koch. Universal gates for protected superconducting qubits using optimal control. *Physical Review A*, 101(2):022321, 2020.
- [2] Konstantin Andreev and Harald Racke. Balanced graph partitioning. *Theory of Computing Systems*, 39(6):929–939, 2006.
- [3] MD SAJID ANIS, Héctor Abraham, AduOffei, Rochisha Agarwal, Gabriele Agliardi, Merav Aharoni, Ismail Yunus Akhalwaya, Gadi Aleksandrowicz, Thomas Alexander, Matthew Amy, Sashwat Anagolum, Eli Arbel, Abraham Asfaw, Anish Athalye, Artur Avkhadiev, Carlos Azaustre, Abhik Banerjee, Santanu Banerjee, Will Bang, Aman Bansal, Panagiotis Barkoutsos, Ashish Barnawal, George Barron, George S. Barron, Luciano Bello, Yael Ben-Haim, Daniel Bevenius, Dhruv Bhatnagar, Arjun Bhoje, Paolo Bianchini, Lev S. Bishop, Carsten Blank, Sorin Bolos, Soham Bopardikar, Samuel Bosch, Sebastian Brandhofer, Brandon, Sergey Bravyi, Nick Bronn, Bryce-Fuller, David Bucher, Artemiy Burov, Fran Cabrera, Padraic Calpin, Lauren Capelluto, Jorge Carballo, Ginés Carrascal, Adam Carriker, Ivan Carvalho, Adrian Chen, Chun-Fu Chen, Edward Chen, Jielun (Chris) Chen, Richard Chen, Franck Chevallier, Rathish Cholarajan, Jerry M. Chow, Spencer Churchill, Christian Claus, Christian Clauss, Caleb Clothier, Romilly Cocking, Ryan Cocuzzo, Jordan Connor, Filipe Correa, Abigail J. Cross, Andrew W. Cross, Simon Cross, Juan Cruz-Benito, Chris Culver, Antonio D. Córcoles-Gonzales, Navaneeth D, Sean Dague, Tareq El Dandachi, Animesh N Dangwal, Jonathan Daniel, Marcus Daniels, Matthieu Dartiailh, Abdón Rodríguez Davila, Faisal Debouni, Anton Dekusar, Amol Deshmukh, Mohit Deshpande, Delton Ding, Jun Doi, Eli M. Dow, Eric Drechsler, Eugene Dumitrescu, Karel Dumon, Ivan Duran, Kareem EL-Safty, Eric Eastman, Grant Eberle, Amir Ebrahimi, Pieter Eendebak, Daniel Egger, Alberto Espiricueta, Mark Everitt, Davide Facchetti, Farida, Paco Martín Fernández, Samuele Ferracin, Davide Ferrari, Axel Hernández Ferrera, Romain Fouilland, Albert Frisch, Andreas Fuhrer, Bryce Fuller, MELVIN GEORGE, Julien Gacon, Borja Godoy Gago, Claudio Gambella, Jay M. Gambetta, Adhisha Gammanpila, Luis Garcia, Tanya Garg, Shelly Garion, Tim Gates, Leron Gil, Austin Gilliam, Aditya Giridharan, Juan Gomez-Mosquera, Gonzalo, Salvador de la Puente González, Jesse Gorzinski, Ian Gould, Donny Greenberg, Dmitry Grinko, Wen Guan, John A. Gunnels, Naman Gupta, Jakob M. Günther, Mikael Haglund, Isabel Haide, Ikko Hamamura, Omar Costa Hamido, Frank Harkins, Areeq Hasan, Vojtech Havlicek, Joe Hellmers, Łukasz Herok, Stefan Hillmich, Hiroshi Horii, Connor Howington, Shaohan Hu, Wei Hu, Junye Huang, Rolf Huisman, Haruki Imai, Takashi Imamichi, Kazuaki Ishizaki, Ishwor, Raban Iten, Toshinari Itoko, Ali Javadi, Ali Javadi-Abhari, Wahaj Javed, Madhav Jivrajani, Kiran Johns, Scott Johnstun, Jonathan-Shoemaker, JosDenmark, JoshDumo, John Judge, Tal Kachmann, Akshay Kale, Naoki Kanazawa, Jessica Kane, Kang-Bae, Annanay Kapila, Anton Karazeev, Paul Kassebaum, Josh Kelso, Scott Kelso, Vismai Khanderao, Spencer King, Yuri Kobayashi, Arseny Kovyrshin, Prasad Kumkar, Gawel Kus, Ryan LaRose, Enrique Lacal, Raphaël Lambert, John Lapeyre, Joe Latone, Scott Lawrence, Christina Lee, Gushu Li, Jake Lishman, Dennis Liu, Peng Liu, Yunho Maeng, Saurav Maheshkar, Kahan Majmudar, Aleksei Malyshv, Mohamed El Mandouh, Joshua Manela, Manjula, Jakub Marecek, Manoel Marques, Kunal Marwaha, Dmitri Maslov, Paweł Maszota, Dolph Mathews, Atsushi Matsuo, Farai Mazhandu, Doug McClure, Maureen McElaney, Cameron McGarry, David McKay, Dan McPherson, Srujan Meesala, Dekel Meirum, Corey Mendell, Thomas Metcalfe, Martin Mevissen, Andrew Meyer, Antonio Mezzacapo, Rohit Midha, Zlatko Minev, Abby Mitchell, Nikolaj Moll, Alejandro Montanez, Gabriel Monteiro, Michael Duane Mooring, Renier Morales, Niall Moran, David Morcuende, Seif Mostafa, Mario Motta, Romain Moyard, Prakash Murali, Jan Müggenburg, David Nadlinger, Ken Nakanishi, Giacomo Nannicini, Paul Nation, Edwin Navarro, Yehuda Naveh, Scott Wyman Neagle, Patrick Neuweiler, Aziz Ngoueya, Johan Nicander, Nick-Singstock, Pradeep Niroula, Hassi Norlen, NuoWenLei, Lee James O’Riordan, Oluwatobi Ogunbayo, Pauline Ollitrault, Tamiya Onodera, Raul Otaolea, Steven Oud, Dan Padilha, Hanhee Paik, Soham Pal, Yuchen Pang, Ashish Panigrahi, Vincent R. Pascuzzi, Simone Perriello, Eric Peterson, Anna Phan, Francesco Piro, Marco Pistoia, Christophe Piveteau, Julia Plewa, Pierre Pocreau, Alejandro Pozas-Kerstjens, Rafał Pracht, Milos Prokop, Viktor Prutyaynov, Sumit Puri, Daniel Puzzuoli, Jesús Pérez, Quintiii, Rafey Iqbal Rahman, Arun Raja, Roshan Rajeev, Nipun Ramagiri, Anirudh Rao, Rudy Raymond, Oliver Reardon-Smith, Rafael Martín-Cuevas Redondo, Max Reuter, Julia Rice, Matt Riedemann, Drew Risinger, Marcello La Rocca, Diego M.

- Rodríguez, Rohith Karur, Ben Rosand, Max Rossmannek, Mingi Ryu, Tharmashastha SAPV, Arijit Saha, Abdullah Ash-Saki, Martin Sandberg, Hirmay Sandesara, Ritvik Sapra, Hayk Sargsyan, Aniruddha Sarkar, Ninad Sathaye, Bruno Schmitt, Chris Schnabel, Zachary Schoenfeld, Travis L. Scholten, Eddie Schoute, Mark Schulterbrandt, Joachim Schwarm, James Seaward, Sergi, Ismael Faro Sertage, Kanav Setia, Freya Shah, Nathan Shammah, Rohan Sharma, Yunong Shi, Jonathan Shoemaker, Adenilton Silva, Andrea Simonetto, Divyanshu Singh, Parmeet Singh, Phattharaporn Singkanipa, Yukio Siraichi, Siri, Jesús Sistos, Iskandar Sitdikov, Seyon Sivarajah, Magnus Berg Sletfjerding, John A. Smolin, Mathias Soeken, Igor Olegovich Sokolov, Igor Sokolov, Soolu Thomas, Starfish, Dominik Steenken, Matt Stypulkoski, Adrien Suau, Shaojun Sun, Kevin J. Sung, Makoto Suwama, Oskar Słowik, Hitomi Takahashi, Tanvesh Takawale, Ivano Tavernelli, Charles Taylor, Pete Taylour, Soolu Thomas, Mathieu Tillet, Maddy Tod, Miroslav Tomasik, Enrique de la Torre, Juan Luis Sánchez Toural, Kenso Trabing, Matthew Treinish, Dimitar Trenev, TrishaPe, Felix Truger, Georgios Tsilimigkounakis, Davindra Tulsi, Wes Turner, Yotam Vaknin, Carmen Recio Valcarce, Francois Varchon, Adish Vartak, Almudena Carrera Vazquez, Prajjwal Vijaywargiya, Victor Villar, Bhargav Vishnu, Desiree Vogt-Lee, Christophe Vuillot, James Weaver, Johannes Weidenfeller, Rafal Wieczorek, Jonathan A. Wildstrom, Jessica Wilson, Erick Winston, WinterSoldier, Jack J. Woehr, Stefan Woerner, Ryan Woo, Christopher J. Wood, Ryan Wood, Steve Wood, James Wootton, Matt Wright, Bo Yang, Daniyar Yeralin, Ryota Yonekura, David Yonge-Mallo, Richard Young, Jessie Yu, Lebin Yu, Christopher Zachow, Laura Zdanski, Helena Zhang, Christa Zoufal, aeddins ibm, alexzhang13, b63, bartek bartlomiej, bcamorrison, brandhsn, catornow, charmerDark, deeplokhande, dekel.meirom, dime10, ehchen, fanizzamarco, fs1132429, gadial, galeinston, georgezhou20, georgios ts, gruu, hhorii, hykavitha, itoko, jliu45, jscott2, klinvill, krutik2966, ma5x, michelle4654, msuwama, ngtiwsvp, ordmoj, sagar pahwa, pritamsinha2304, ryancocuzzo, saswati qiskit, septembr, sethmerkel, shaashwat, sternparky, strickroman, tigerjack, tsura crisaldo, welien, willhbang, yang.luh, and Mantas Čepulkovskis. Qiskit: An open-source framework for quantum computing, 2021.
- [4] Frank Arute, Kunal Arya, Ryan Babbush, Dave Bacon, Joseph C Bardin, Rami Barends, Rupak Biswas, Sergio Boixo, Fernando GSL Brandao, David A Buell, et al. Quantum supremacy using a programmable superconducting processor. *Nature*, 574(7779):505–510, 2019.
- [5] Adriano Barenco, Artur Ekert, Kalle-Antti Suominen, and Päivi Törmä. Approximate quantum fourier transform and decoherence. *Physical Review A*, 54(1):139, 1996.
- [6] Ethan Bernstein and Umesh Vazirani. Quantum complexity theory. *SIAM Journal on computing*, 26(5):1411–1473, 1997.
- [7] Sergio Boixo, Sergei V Isakov, Vadim N Smelyanskiy, Ryan Babbush, Nan Ding, Zhang Jiang, Michael J Bremner, John M Martinis, and Hartmut Neven. Characterizing quantum supremacy in near-term devices. *Nature Physics*, 14(6):595–600, 2018.
- [8] Sergey Bravyi, Guillaume Duclos-Cienci, David Poulin, and Martin Suchara. Subsystem surface codes with three-qubit check operators. *arXiv preprint arXiv:1207.1443*, 2012.
- [9] Sergey Bravyi, Graeme Smith, and John A Smolin. Trading classical and quantum computational resources. *Physical Review X*, 6(2):021043, 2016.
- [10] Zhao-Yun Chen, Qi Zhou, Cheng Xue, Xia Yang, Guang-Can Guo, and Guo-Ping Guo. 64-qubit quantum circuit simulation. *Science Bulletin*, 63(15):964–971, 2018.
- [11] Yongshan Ding, Pranav Gokhale, Sophia Fuhui Lin, Richard Rines, Thomas Propson, and Frederic T Chong. Systematic crosstalk mitigation for superconducting qubits via frequency-aware compilation. In *2020 53rd Annual IEEE/ACM International Symposium on Microarchitecture (MICRO)*, pages 201–214. IEEE, 2020.
- [12] Andrew Eddins, Mario Motta, Tanvi P Gujarati, Sergey Bravyi, Antonio Mezzacapo, Charles Hadfield, and Sarah Sheldon. Doubling the size of quantum simulators by entanglement forging. *arXiv preprint arXiv:2104.10220*, 2021.
- [13] Edward Farhi, Jeffrey Goldstone, and Sam Gutmann. A quantum approximate optimization algorithm. *arXiv preprint arXiv:1411.4028*, 2014.
- [14] Austin G Fowler, Matteo Mariantoni, John M Martinis, and Andrew N Cleland. Surface codes: Towards practical large-scale quantum computation. *Physical Review A*, 86(3):032324, 2012.
- [15] Johnnie Gray and Stefanos Kourtis. Hyper-optimized tensor network contraction. *Quantum*, 5:410, 2021.

- [16] Lov K Grover. A fast quantum mechanical algorithm for database search. In *Proceedings of the twenty-eighth annual ACM symposium on Theory of computing*, pages 212–219, 1996.
- [17] Gurobi Optimization, LLC. Gurobi optimizer reference manual, 2021.
- [18] Thomas Häner and Damian S Steiger. 0.5 petabyte simulation of a 45-qubit quantum circuit. In *Proceedings of the International Conference for High Performance Computing, Networking, Storage and Analysis*, pages 1–10, 2017.
- [19] Ali Javadi-Abhari, Pranav Gokhale, Adam Holmes, Diana Franklin, Kenneth R Brown, Margaret Martonosi, and Frederic T Chong. Optimized surface code communication in superconducting quantum computers. In *Proceedings of the 50th Annual IEEE/ACM International Symposium on Microarchitecture*, pages 692–705, 2017.
- [20] PV Klimov, Julian Kelly, Z Chen, Matthew Neeley, Anthony Megrant, Brian Burkett, Rami Barends, Kunal Arya, Ben Chiaro, Yu Chen, et al. Fluctuations of energy-relaxation times in superconducting qubits. *Physical review letters*, 121(9):090502, 2018.
- [21] Daniel Litinski. A game of surface codes: Large-scale quantum computing with lattice surgery. *Quantum*, 3:128, 2019.
- [22] Yong Liu, Xin Liu, Fang Li, Haohuan Fu, Yuling Yang, Jiawei Song, Pengpeng Zhao, Zhen Wang, Dajia Peng, Huarong Chen, et al. Closing the “quantum supremacy” gap: achieving real-time simulation of a random quantum circuit using a new sunway supercomputer. In *Proceedings of the International Conference for High Performance Computing, Networking, Storage and Analysis*, pages 1–12, 2021.
- [23] Igor L Markov and Yaoyun Shi. Simulating quantum computation by contracting tensor networks. *SIAM Journal on Computing*, 38(3):963–981, 2008.
- [24] Pranav Mundada, Gengyan Zhang, Thomas Hazard, and Andrew Houck. Suppression of qubit crosstalk in a tunable coupling superconducting circuit. *Physical Review Applied*, 12(5):054023, 2019.
- [25] Prakash Murali, Jonathan M Baker, Ali Javadi-Abhari, Frederic T Chong, and Margaret Martonosi. Noise-adaptive compiler mappings for noisy intermediate-scale quantum computers. In *Proceedings of the Twenty-Fourth International Conference on Architectural Support for Programming Languages and Operating Systems*, pages 1015–1029, 2019.
- [26] Prakash Murali, David C McKay, Margaret Martonosi, and Ali Javadi-Abhari. Software mitigation of crosstalk on noisy intermediate-scale quantum computers. In *Proceedings of the Twenty-Fifth International Conference on Architectural Support for Programming Languages and Operating Systems*, pages 1001–1016, 2020.
- [27] Giacomo Nannicini, Lev S Bishop, Oktay Gunluk, and Petar Jurcevic. Optimal qubit assignment and routing via integer programming. *arXiv preprint arXiv:2106.06446*, 2021.
- [28] Román Orús. A practical introduction to tensor networks: Matrix product states and projected entangled pair states. *Annals of Physics*, 349:117–158, 2014.
- [29] Edwin Pednault, John A Gunnels, Giacomo Nannicini, Lior Horesh, and Robert Wisnieff. Leveraging secondary storage to simulate deep 54-qubit sycamore circuits. *arXiv preprint arXiv:1910.09534*, 2019.
- [30] Tianyi Peng, Aram W Harrow, Maris Ozols, and Xiaodi Wu. Simulating large quantum circuits on a small quantum computer. *Physical Review Letters*, 125(15):150504, 2020.
- [31] Neil Robertson and Paul D Seymour. Graph minors. x. obstructions to tree-decomposition. *Journal of Combinatorial Theory, Series B*, 52(2):153–190, 1991.
- [32] Zain H Saleem, Teague Tomesh, Bilal Tariq, and Martin Suchara. Approaches to constrained quantum approximate optimization. *arXiv preprint arXiv:2010.06660*, 2020.
- [33] Ulrich Schollwöck. The density-matrix renormalization group in the age of matrix product states. *Annals of physics*, 326(1):96–192, 2011.
- [34] Peter W Shor. Polynomial-time algorithms for prime factorization and discrete logarithms on a quantum computer. *SIAM review*, 41(2):303–332, 1999.
- [35] Martin Suchara, Arvin Faruque, Ching-Yi Lai, Gerardo Paz, Frederic T Chong, and John Kubiatowicz. Comparing the overhead of topological and concatenated quantum error correction. *arXiv preprint arXiv:1312.2316*, 2013.
- [36] Bochen Tan and Jason Cong. Optimality study of existing quantum computing layout synthesis tools. *IEEE Transactions on Computers*, 2020.
- [37] Wei Tang and Margaret Martonosi. Cutting quantum circuits to run on quantum and classical platforms. *arXiv preprint arXiv:2205.05836*, 2022.

- [38] Wei Tang, Teague Tomesh, Martin Suchara, Jeffrey Larson, and Margaret Martonosi. Cutqc: using small quantum computers for large quantum circuit evaluations. In *Proceedings of the 26th ACM International Conference on Architectural Support for Programming Languages and Operating Systems*, pages 473–486, 2021.
- [39] Teague Tomesh, Pranav Gokhale, Eric R Anschuetz, and Frederic T Chong. Coreset clustering on small quantum computers. *Electronics*, 10(14):1690, 2021.
- [40] Frank Verstraete, Juan J Garcia-Ripoll, and Juan Ignacio Cirac. Matrix product density operators: Simulation of finite-temperature and dissipative systems. *Physical review letters*, 93(20):207204, 2004.
- [41] Guifré Vidal. Efficient classical simulation of slightly entangled quantum computations. *Physical review letters*, 91(14):147902, 2003.
- [42] Guifré Vidal. Efficient simulation of one-dimensional quantum many-body systems. *Physical review letters*, 93(4):040502, 2004.
- [43] Xin-Chuan Wu, Sheng Di, Emma Maitreyee Dasgupta, Franck Cappello, Hal Finkel, Yuri Alexeev, and Frederic T Chong. Full-state quantum circuit simulation by using data compression. In *Proceedings of the International Conference for High Performance Computing, Networking, Storage and Analysis*, pages 1–24, 2019.
- [44] Xanadu. Xanadu awarded darpa grant to develop novel quantum compiler for nisq-based machines, 2021. <https://www.prnewswire.com/news-releases/xanadu-awarded-darpa-grant-to-develop-novel-quantum-compiler-for-nisq-based-machines-301337111.html>.
- [45] Theodore J Yoder and Isaac H Kim. The surface code with a twist. *Quantum*, 1:2, 2017.
- [46] Xiao Yuan, Jinzhao Sun, Junyu Liu, Qi Zhao, and You Zhou. Quantum simulation with hybrid tensor networks. *Physical Review Letters*, 127(4):040501, 2021.